東京大学 大学院新領域創成科学研究科

物質系専攻

2021 年度

修士論文

NMR studies of non-centrosymmetric phases in the spin-orbit coupled metal $Cd_2Re_2O_7$

NMR によるスピン軌道結合金属 $Cd_2Re_2O_7$ の非反転対称相の研究

2021 年 **1**月 **18** 日提出

指導教員 瀧川 仁 教授

夏 靖丁

NMR studies of non-centrosymmetric phases

in the spin-orbit coupled metal $Cd_2Re_2O_7$

Contents

Chapter.1

General Introduction

1 .1 Introduction

There has been increasing interest in novel phenomena caused by strong spin-orbit coupling in metals which do not have inversion symmetry. In such materials, spin degeneracy of the conduction electrons is lifted even without magnetic order. This results in spin-split energy bands and spin-polarized Fermi surfaces, which may cause unusual magneto-current effects and non-reciprocal transport in magnetic fields.

According to this, this lecture is to do the research of Pyrochlore oxide. Pyrochlore oxide is a transition metal oxide represented by the general formula $A_2B_2O_7$, and its crystal structure is composed of BO_6 octahedron and a three-dimensional network of A and oxygen as shown in **Fig.1.1**In such materials, spin degeneracy of the conduction electrons is lifted even without magnetic order.

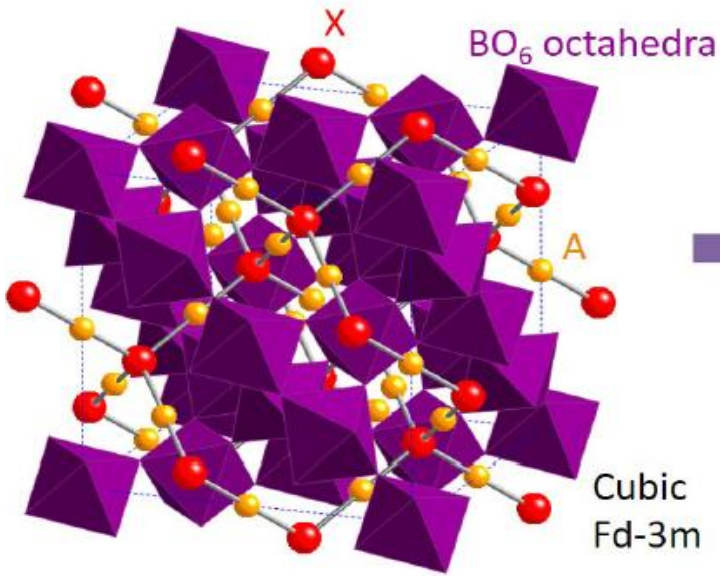

This results in spin-split energy bands and spin-polarized Fermi surfaces, which may cause unusual magneto-current effects and non-reciprocal transport in magnetic fields. Research on the magnetism of pyrochlore oxide is gradually increasing.[1]

$Cd_2Re_2O_7$ is the only superconductor among the pyrochlore oxides represented by the chemical formula $A_2B_2O_7$.[2,3,4] Since 2001, when superconductivity was discovered.

Its superconducting state and structural phase transition have been enthusiastically studied. Some interesting phenomena have been identified, such as the structural phase transition that breaks the inversion symmetry at 200 K and the structural phase transition that does not reduce the symmetry at 120 K.

1.2 $Cd_2Re_2O_7$

$Cd_2Re_2O_7$ is a metallic pyrochlore compound, in which both Cd and Re atoms form a network of corner sharing tetrahedra are known as the pyrochlore lattice. It exhibits sequential phase transitions as a function of temperature. At T_{s1}~200 K, the space group of the crystal structure changes from the high-temperature cubic $Fd\bar{3}m$ to the low-temperature tetragonal $I\bar{4}m2$, which breaks inversion symmetry. At T_{s2}~110 K, the second transition takes place from $I\bar{4}m2$ to another tetragonal and non-centrosymmetric $I4_122$ structure [5,6]. Although the changes in the lattice parameters are extremely small across these transitions, of the order of 10^{-4}, electronic properties such as resistivity and magnetic susceptibility show pronounced anomalies at T_{s1} and T_{s2}. This suggests that the phase transitions in $Cd_2Re_2O_7$ are driven by electronic instability not by lattice instability.

In recent research, Lian Fu proposed theoretically that interacting electrons with strong spin-orbit coupling may break inversion symmetry spontaneously, leading to orders of odd-parity multipole moments [7]. Hayami et al. pointed out that the structural changes mentioned above are compatible with order of electric toroidal quadrupoles with E_u symmetry [8].

1.3 Basic Physical Properties And Structural Phase Transition

The Electrical resistance and the temperature dependence of magnetic susceptibility about $Cd_2Re_2O_7$ is shown in **Fig.1.2** and **Fig.1.3.**

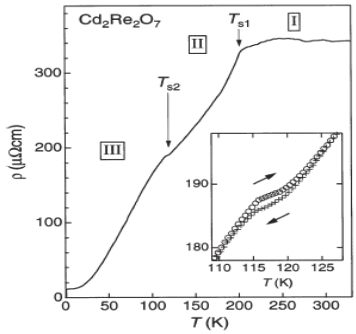

Fig.1.2. Temperature dependence of Electrical resistance [2]

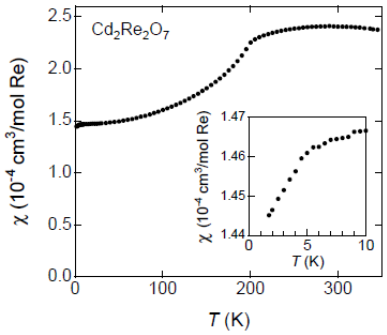

Fig.1.3 Temperature dependence of magnetic susceptibility [9]

Anomalies corresponding to structural phase transitions are observed in electrical resistance measurements. When cooling from 300 K, at Ts1~200 K, the space group of the crystal structure changes from the high-temperature cubic to the low temperature tetragonal, which breaks inversion symmetry. AtTs2~120 K, the second transition takes place from $I\bar{4}m2$ to $I4_122$, which is also a tetragonal crystal. These three phases are called the phase I, phase II, and phase III from the high-temperature phase, respectively, shown as **Fig1.4**[5,10]

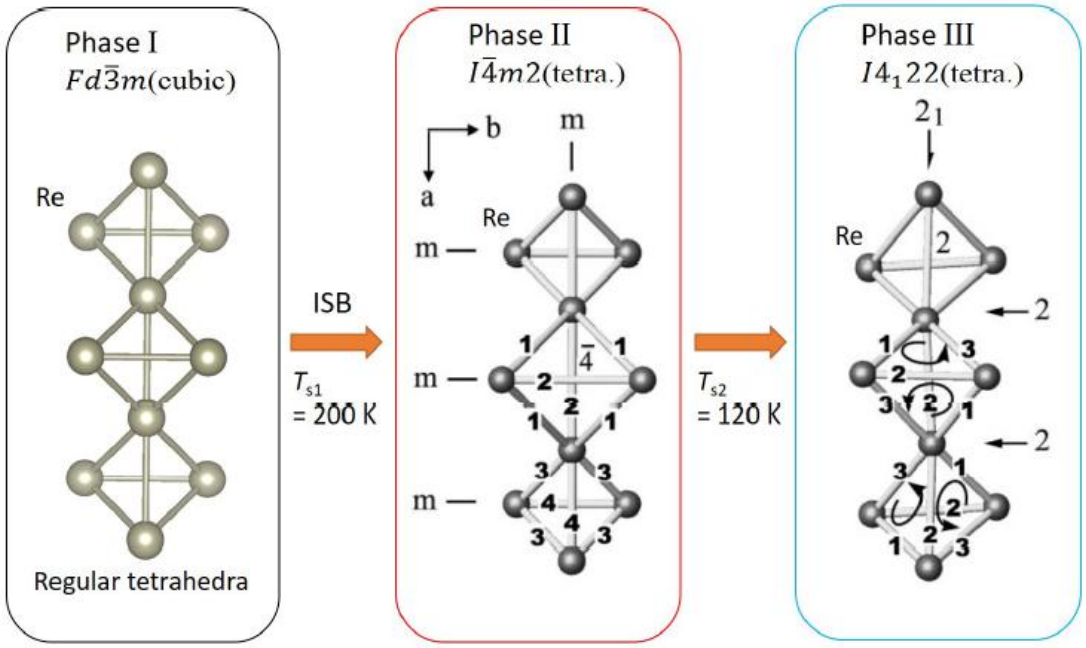

Fig.1.4 Structural phase transition of Cd2Re2O7 focusing on Re site

And **Fig.1.5**[6] shows the temperature dependence of electrical resistance measured using a single crystal.

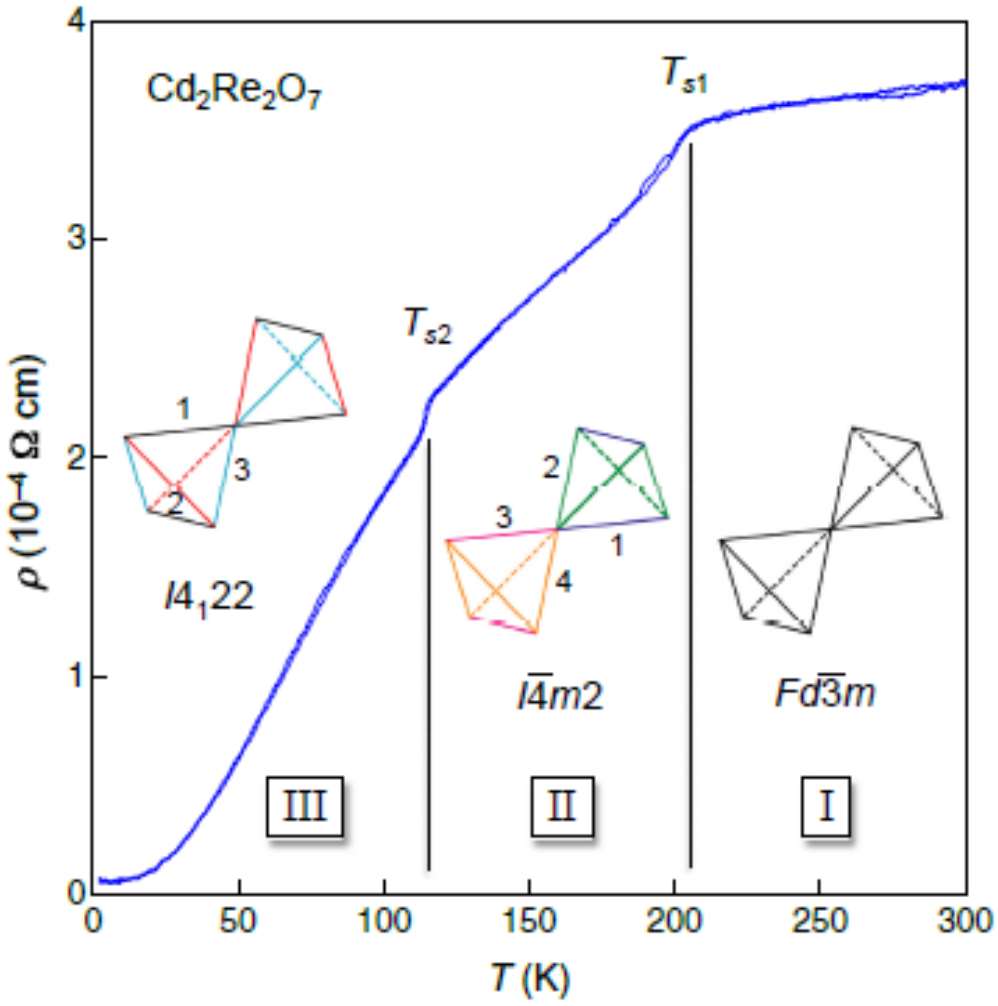

Fig.1.5 Structure transition of $Cd_2Re_2O_7$ [6]

At Ts1 = 205 K and Ts2 = 112 K, the temperature gradient of electrical resistance changes significantly. The pyrochlore lattice formed by Re (Cd) is shown in the figure, but the Re-Re (Cd-Cd) bond, which was equivalent in phase I, changed to four types that were not equivalent in phase II, and the two tetrahedra were It becomes unequal. This is due to the disappearance of the 3-fold axis in Phase II. In Phase III, the mirror surface is replaced by a double axis, so he has three types of unequal bonds, and the two tetrahedra become equivalent again. In Phase II and Phase III, three types of domains with different axial directions are formed by tetragonal distortion. [6]

Structural parameters

	X	Y	Z	Wyckoff Position
A	0.5	0.5	0.5	16d
B	0	0	0	16c
O	X	0.125	0.125	48f
O’	0.375	0.375	0.375	8b

1.4 Transition of Ts1

Inversion symmetry breaking (ISB) is that during the phase transition, inversion symmetry is broken.

The Fig.1.3 shows the temperature dependence of the magnetic susceptibility of $Cd_2Re_2O_7$.The magnetic susceptibility of paramagnetic metals is mainly given by Pauli paramagnetic χ Pauli shown in the following equation

$$\chi\text{Pauli} = \frac{1}{4} g^2 \mu_B{}^2 D(E_F) \qquad (1)$$

where g is the g value, μ_B is the Bohr magneton, and D (E_F) is the density of states in Fermi energy.

From the above equation, it can be seen that the transition of $Ts1$ may lead to a decrease in the density of states in Fermi energy.

Inversion symmetry breaking (ISB) transitions are universal in insulators and are found in ferroelectrics and pyroelectrics. The ISB transition of an insulator is driven by an electrical dipole-dipole interaction, but in metallic systems such as

Cd2Re2O7, such long-range Coulomb interactions are shielded by itinerant electrons. Therefore, it is necessary to consider another phase transition mechanism.

Landau's theory expands the free energy by order parameters and captures the phase transition phenomena logically. The structural phase transition of $Cd_2Re_2O_7$ has been interpreted using Landau theory [12,13]. Fig.1.6[5] shows the group-subgroup relationship for $Fd\bar{3}m$. And Eu mode is a strange symmetry mode, which breaks the inversion symmetry, and when it freezes, the inversion symmetry of the crystal is lost. According to Landau's theory, it is expected that the ratio of a-axis length to c-axis length is reversed between phase II and phase III [13].

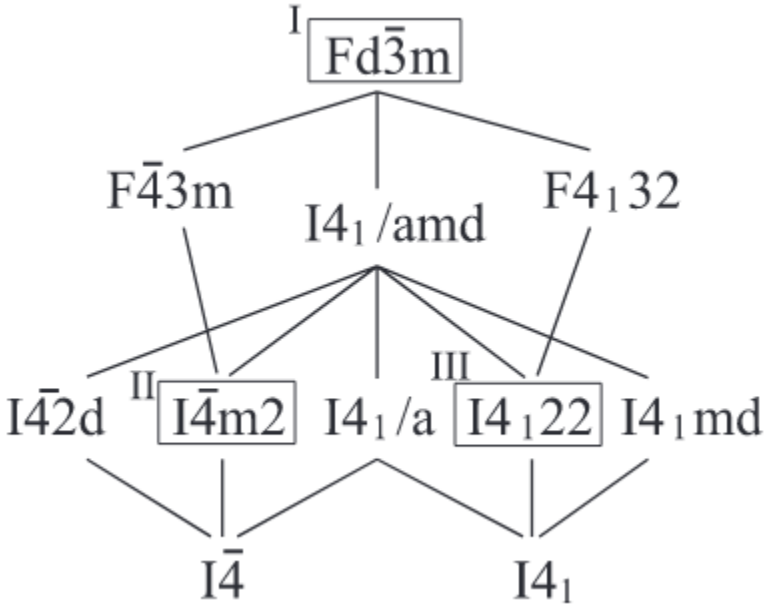

Fig1.6 Group-subgroup relations of Space group[5]

Chapter.2

NMR Nuclear Magnetic Resonance

NMR is an abbreviation for Nuclear Magnetic Resonance, which means observing the resonance phenomenon of nuclear spins. It is a way to know the state of an electron through the interaction between the nucleus and surrounding electrons. The Zeeman splitting of spin energy level occurs in the nucleus with nonzero magnetic moment under the action of an external magnetic field, and the resonance absorption of a certain frequency of radiofrequency radiation.

2.1 NMR Resonance Absorption

The magnetic moment of the nucleus is given as

$$\boldsymbol{\mu}=g_{\mathrm{N}}\mu_N\boldsymbol{I} \qquad (2)$$

$$=\gamma\hbar\boldsymbol{I}$$

where $g_{\mathrm{N\,is}}$ g factor of the nucleus, μ_N=0.5×10−24 ergOe-1 , γ is the gyromagnetic ratio.

Applied a static magnetic field $\mathcal{H}_0$ to this system in the z-direction, the Hamiltonian for nuclear spins is given as:

$$\mathcal{H}_0=-\boldsymbol{\mu}\cdot\boldsymbol{H_0}=-\gamma\hbar\boldsymbol{I}\cdot\boldsymbol{H_0} \qquad (3)$$

And Energy eigenvalue is given as:

$$E_m=-\gamma\hbar H_0 m \quad (m=-I,-I+1,\ldots,I) \qquad (4)$$

which divided into 2L + 1

The intervals between these energy levels are equal intervals of $\triangle E = \gamma\hbar Hz$. When a vibrating magnetic field with a frequency satisfying Δ E =$\hbar\omega$ is applied

from the direction perpendicular to the static magnetic field, a transition occurs between the above levels, and magnetic resonance can be observed.

In fact, nuclear spins have electrical and magnetic hyperfine interactions with surrounding electrons and ions. Through these interactions, NMR measurements can provide information about local electronic states for specific nuclei in matter.

2.2 Hyperfine Interaction

Hyperfine interactions are working between the nucleus and the surrounding electrons. There are two types of this interaction: electrical nuclear quadrupole interaction and magnetic hyperfine interaction. In NMR measurement, it is possible through this interaction to obtain static and dynamic information of the electronic system. Here we focus on the magnetic hyperfine interaction, which causes the NMR resonance lines to shift, creating an internal magnetic field in a magnetically ordered state.

Takes the nucleus as the origin, when the nuclear magnetic moment exists as $\boldsymbol{\mu}_n=\gamma_n\hbar\boldsymbol{I}$.

The electron exists at a position $\boldsymbol{r}$, the vector potential created by the electron p osition is given as:

$$\boldsymbol{A}(\boldsymbol{r})=\boldsymbol{\nabla}\times\frac{\mu n}{\gamma} \qquad (5)$$

The interaction between $\boldsymbol{A}$ $(\boldsymbol{r})$ and electrons is given as H1

$$\mathcal{H}1=\frac{1}{2m}(\boldsymbol{p}+\frac{e}{c}\boldsymbol{A})^2+2\mu_B\boldsymbol{s}\cdot\nabla\times\boldsymbol{A} \qquad (6)$$

where m is Electron mass, μ_B is Bohr magneton.

When $\boldsymbol{A}$ $(\boldsymbol{r})=0$, the $\mathcal{H}1$ is given as:

$$\mathcal{H}1=\frac{e}{2mc}(\boldsymbol{p}\cdot\boldsymbol{A}+\boldsymbol{A}\cdot\boldsymbol{p}+\frac{e}{c}\boldsymbol{A}^2)+2\mu_B\boldsymbol{s}\cdot\nabla\times\boldsymbol{A}$$

$$=\mathcal{H}l+\mathcal{H}s+\frac{e^2}{2mc^2}\boldsymbol{A}^2 \qquad (7)$$

Here, the first term $\mathcal{H}\iota$ is the interaction between the nuclear spin and the orbital angular momentum, and the second term $\mathcal{H}s$ is the interaction between the nuclear spin and the electron spin.

For $\nabla\times\frac{\mu n}{r}=\frac{\mu n\times r}{r^3}$, $\mathcal{H}\iota$ is given as:

$$\mathcal{H}\iota=2\mu_B\frac{l\cdot\mu n}{r^3} \qquad (8)$$

For $\boldsymbol{\nabla}\times\boldsymbol{\nabla}\times\frac{\mu n}{r}=\boldsymbol{\nabla}\boldsymbol{\nabla}\cdot\frac{\mu n}{r}-\Delta\frac{\mu n}{r}$

The interaction between nuclear spins and electron spins $\mathcal{H}s$ is given as

$$\mathcal{H}s=2\mu_B[(\boldsymbol{s}\cdot\boldsymbol{\nabla})(\boldsymbol{\mu n}\cdot\boldsymbol{\nabla})\frac{1}{r}-\frac{1}{3}\boldsymbol{s}\cdot\Delta\frac{\mu n}{r}]-\frac{4}{3}\mu B\boldsymbol{s}\cdot\Delta\frac{\mu n}{r} \qquad (9)$$

when $r\neq 0$, The first term magnetic dipole interaction $\mathcal{H}dip$ is

$$\mathcal{H}dip=-\frac{2\mu_B s\cdot\mu n}{r3}+\frac{3(2\mu_B s\cdot r)(\mu n\cdot r)}{r5} \qquad (10)$$

On the other hand, when $r\to 0$, the first term disappears, where $\Delta\frac{1}{r}=-4\pi\delta(r)$, and the Fermi contact interaction is given as:

$$\mathcal{H}F=\frac{16}{3}\pi\mu_B s\cdot\mu n\,\delta(r) \qquad (11)$$

the magnetic field of hyperfine interaction H_{hf} is given as

$$\mathcal{H}_{hf}=\mathcal{H}s+\mathcal{H}dip+\mathcal{H}F \qquad (12)$$

2.3 Electric Quadrupole Interaction

The splitting of energy levels may be due to electrical as well as magnetic fields. When the nuclear spin $I\geq 1$, the charge distribution of the nucleus is not completely spherically symmetric, but a spheroid with the nuclear spin direction as the z-axis. When such a nucleus is placed in a gradient electric field, the energy of

the nucleus depends on the orientation of the spheroid. The energy level of the nuclear spin will split.

To derived the Hamiltonian of the electric quadrupole interaction, assuming that the origin is located in the center of the atom, Coulomb energy E is given as

$$E=\int \rho(r)V(r)dv \qquad (13)$$

where $\rho(\boldsymbol{r})$ is the electrostatic potential of the atom.

The electrostatic potential V $(\boldsymbol{r})$ expands near the origin is given as

$$V(\boldsymbol{r})=V(0)+\sum_{\mathrm{i}} \mathrm{xi}\left(\frac{\partial \mathrm{V}}{\partial \mathrm{xi}}\right)_{\mathrm{r}=0}+\frac{1}{2}\sum_{\mathrm{i,j}} \mathrm{xixj}\left(\frac{\partial^2 \mathrm{V}}{\partial \mathrm{xi}\,\partial \mathrm{xj})}\right)_{\mathrm{r}=0}+\cdots \qquad (14)$$

So there is

$$\mathrm{E}=V(0)\int \rho(r)dv+\Sigma V_i\int x_i\rho(r)dv+\frac{1}{2}\Sigma V_{ij}\int x_i x_j\rho(r)dv+\ldots \qquad (15)$$

where $\mathrm{Vi}=\left(\frac{\partial \mathrm{V}}{\partial \mathrm{xi}}\right)_{\mathrm{r}=0}$, $\mathrm{Vi,j}=\left(\frac{\partial^2 \mathrm{V}}{\partial \mathrm{xi}\,\partial \mathrm{xj})}\right)_{\mathrm{r}=0}$

The first term gives a constant value. The second term becomes zero because the center of gravity and the center of charge coincide, and the third term represents the quadrupole interaction. Using the Wigner-Eckert theorem, Hamiltonian of electric quadrupole interaction $\mathcal{H}\mathrm{Q}$ is given as

$$\begin{aligned}\mathcal{H}\mathrm{Q}&=\frac{\mathrm{e}^2\mathrm{qQ}}{4\mathrm{I}(2\mathrm{I}-1)}\{(3\mathrm{Iz}^2-\mathrm{I}^2)+\frac{1}{2}\eta(\mathrm{I}_+^2+\mathrm{I}_-^2)\}\\&\equiv\frac{1}{6}hvQ\{(3\mathrm{Iz}^2-\mathrm{I}^2)+\frac{1}{2}\eta(\mathrm{I}_+^2+\mathrm{I}_-^2)\}\end{aligned} \qquad (16)$$

where $eq\equiv Vzz$、$\eta\equiv\frac{\mathrm{Vxx}-\mathrm{Vyy}}{\mathrm{Vzz}}$. Q is the nuclear quadrupole moment and Vzz is the maximum principal axis of the electric field gradient tensor generated at the nuclear position. x, y, z are the main axes of the electric field gradient tensor. Here, Vxx, Vyy, Vzz satisfy the Laplace equation (Vxx + Vyy + Vzz = 0).

2.4 Knight Shift

The shift of the resonance frequency caused by the hyperfine magnetic field is called the Knight shift (K). When the magnetic moment of an electron is oriented in the direction of application of an external magnetic field H_0, the magnetic moment **S** (per 1 μB of one electron) can be written as follows:

$$S = \frac{\chi}{N\mu_B} H_0 \qquad (17)$$

where χ is the magnetic susceptibility of N electrons

Using the magnetic moment S, the hyperfine magnetic field H_{hf} is given as

$$H_{hf} = A.\frac{\chi}{N\mu_B} H_0 \qquad (18)$$

A is the amount of second-order tensors called hyperfine-bonded tensors. Generally, when a substance with a nuclear gyromagnetic ratio γ is placed in an external magnetic field H_0. The resonance frequency ω is given as

$$\begin{aligned} \omega &= \gamma(\omega_0 + \omega_{hf}) \\ &= \gamma(H_0 + H_{hf}) \\ &= \gamma H_0 \left(1 + \frac{H_{hf}}{H_0}\right) \end{aligned} \qquad (19)$$

where $\omega_0 = \gamma_n H_0$ .For here, Knight shift K is given as:

$$K \equiv \frac{H_{hf}}{H_0} \qquad (20)$$

by (19) and (20)， Knight shift is given as:

$$K = A\frac{\chi}{N\mu_B} \qquad (21)$$

It turns out that the measurement of shift is a means to know the local magnetic susceptibility at the nuclear position. The slope of the plot K−χ reflects the hyperfine coupling constant, and static information of the internal magnetic field can be obtained.

2.5 Spin-echo

When a high-frequency magnetic field $\mathbf{H}_1$ is applied to the sample in a pulse shape with a certain time width t, left for a certain time τ, and then a high-frequency magnetic field is applied again with a time width of 2t, which is twice the previous time, a resonance signal is observed after that time 2τ.

Applied an external magnetic field $\mathbf{H}_0$ is in the Z-axis direction, the nuclear magnetization M precesses around the Z-axis at an angular velocity ω.

For here, we consider a coordinate system (x', y', z') that rotates around the Z-axis at an angular velocity ω(a) in **Fig.2.1**. A vibrating magnetic field $\mathbf{H}_1$ (Amplitude H_1, Angular frequency ω) is applied in the X-direction perpendicular to the external magnetic field $\mathbf{H}_0$ until the nuclear magnetization M collapses on the y-axis. When H_1 disappears, lateral relaxation occurs and the nuclear magnetization diffuses axisymmetrically on the x-y plane（b）. The signal observed at this time is called Free Induction Decay (FID).

Furthermore, after this time τ, addition is added again until the magnetization is reversed to the x-axis (c). Magnetization continues to rotate on the x-y plane, gathering on the y-axis after time τ(d , e). The signal observed at this time is a spin echo.

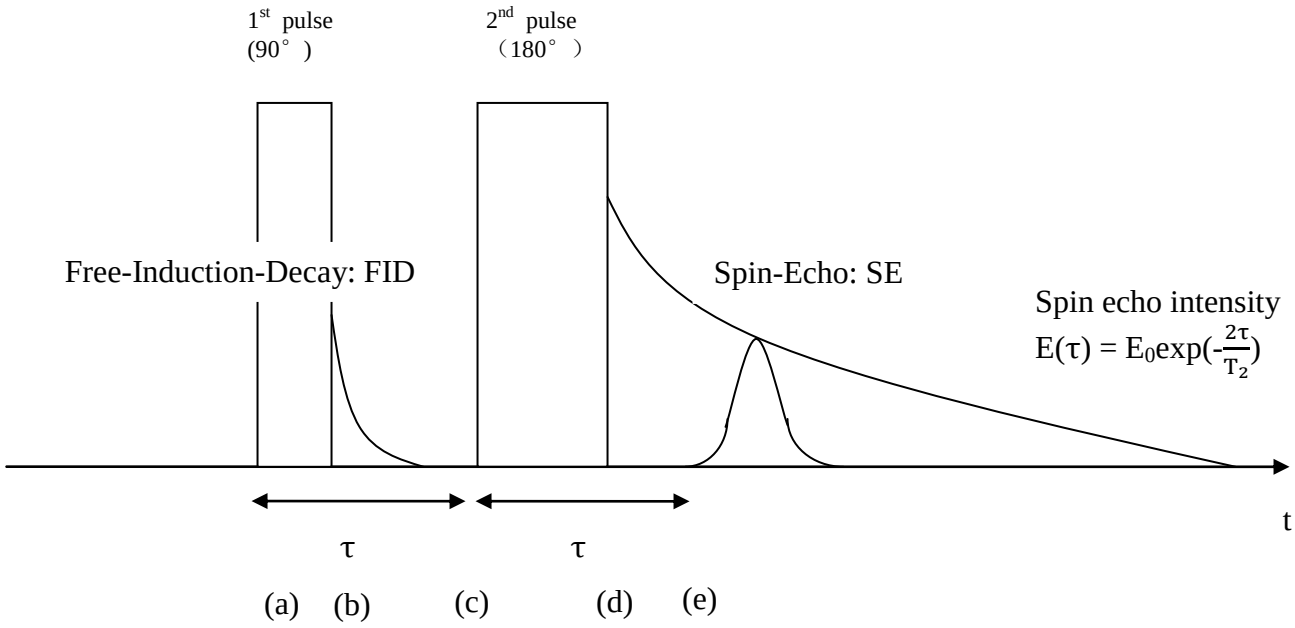

Fig.2.1 Formation and attenuation of FID and SE in the spin echo

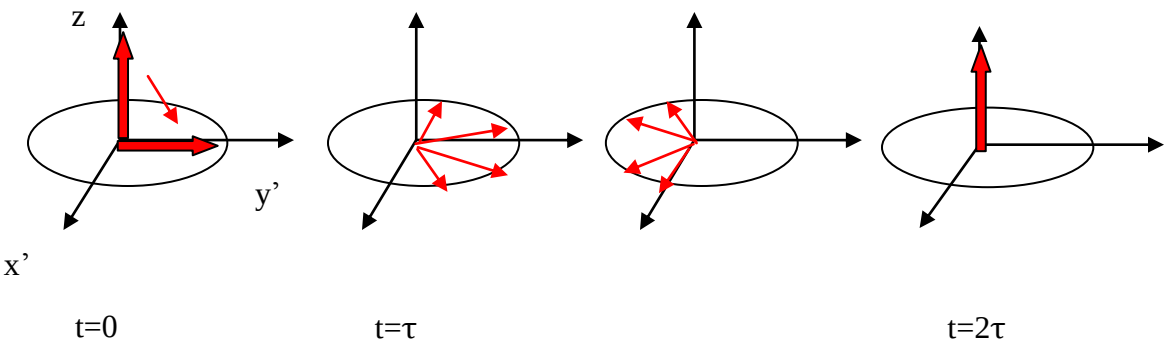

Fig.2.2 Schematic diagram of spin echo

2.6 FT-NMR

As mentioned in the previous section, the reason for the attenuation of FID is the spatial distribution and temporal fluctuation of the magnetic field felt by the nucleus, but the most important of these is the interaction of magnetic dipoles caused by adjacent nuclear spins and the surrounding environment or the generation of surrounding electrons. The local magnetic field (such as Hyperfine magnetic field). One of the main purposes of NMR experiments is to understand the distribution of local magnetic fields. Consider the static distribution of the local magnetic field P(H), where the combined magnetic field of the external magnetic field and the local magnetic field is H, then the FID signal is given as:

$$V(t)=\int P(H)\cos(\gamma Ht)dH \tag{22}$$

This means that FID is represented by the Fourier transform of the local magnetic field distribution, that is, the inverse Fourier transform of FID is obtained. Although the signal needs to be digitized in order to perform the Fourier transform of the FID, since the signal is usually up to 100 MHz, the low-frequency signal obtained by two-phase detection using DBM undergoes a complex Fourier transform to obtain the local magnetic field distribution.

Make H_0 be the center of P(H), which off-center distribution function **h**= $H-H_0$. If the frequency of the oscillating magnetic field is ω_0, then FID is given as:

$$V(t)=\int_{-\infty}^{\infty} \mathrm{p(h)cos(\gamma(H0+h)t)dh} = A(t)\cos(\omega 0t+\psi(t))$$

$$\begin{cases} \mathrm{A(t)cos\psi(t)} = \int_{\infty}^{\infty} \mathrm{p(h)cos(\gamma ht)dh} \\ \mathrm{A(t)sin\psi(t)} = \int_{\infty}^{\infty} \mathrm{p(h)sin(\gamma ht)dh} \end{cases} \tag{23}$$

A(t) and $\psi(t)$ are low frequency components with lower frequencies than ω_0, and two types of low frequency signals with high frequency components cut by DBM is $V_1(t) = A(t)\cos\psi(t) / 2$, $V_2(t)= A(t)\sin\psi(t) / 2$. When these are displayed as a complex number:

$$V_1(t)+iV_2(t)=\int_{-\infty}^{\infty} \mathrm{p(h)exp(-i\gamma ht)dh} \tag{24}$$

The local magnetic field distribution can be obtained by performing a complex Fourier transform on this. The method of obtaining the local magnetic field distribution in this way is called FT NMR, and the obtained local magnetic field distribution is called the NMR spectrum.

2.7 Experimental Device

First, the pulse signal output from the Pulse Generator and the high-frequency signal output from the Signal generator is superposed by the Modulater at the instruction from the computer. After that, the output is adjusted by Attenuater, amplified by Power amp, and sent to the coil. The signal generated by magnetic resonance is amplified by Preamp, mixed with the reference signal by DBM, and phase-detected. The signal after detection is gradually decremented by the Low pass filter and sent to the Oscilloscope. Finally this data will be analyzed with a computer.

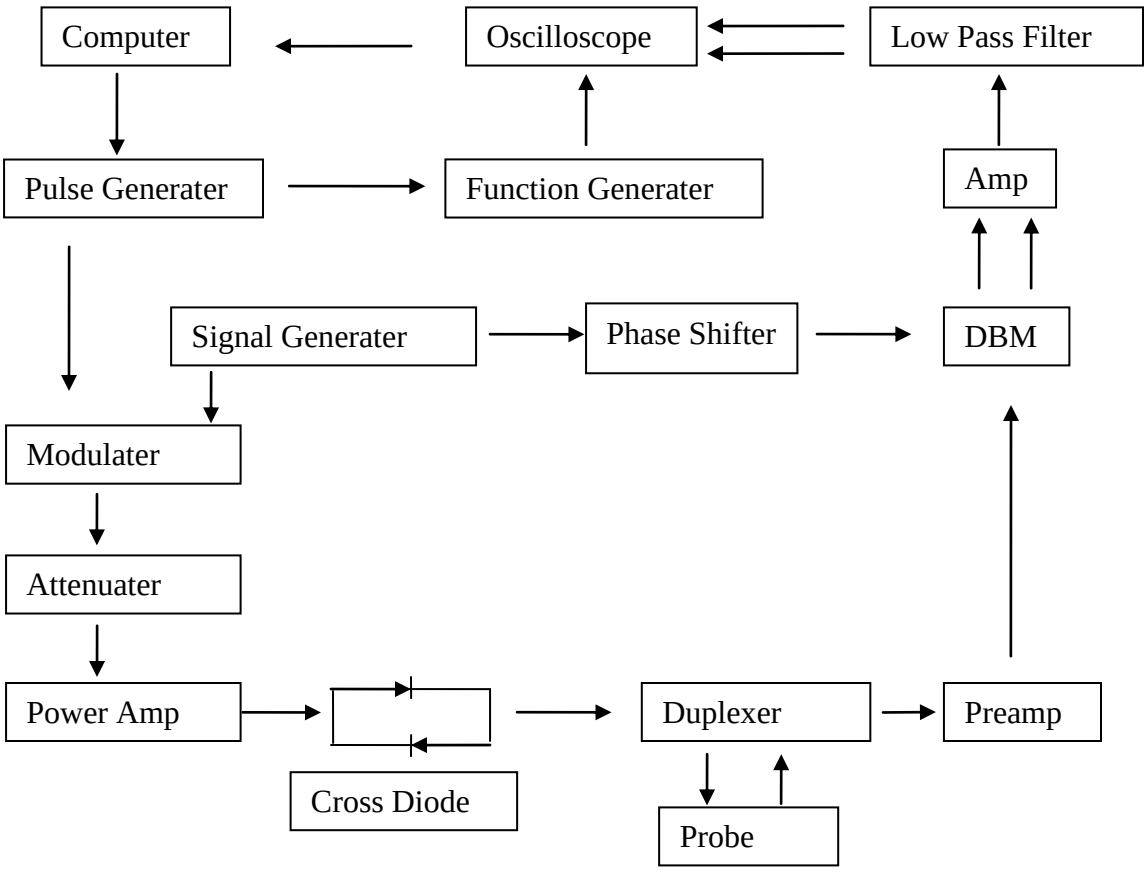

Fig.2.3 **Experimental Device**

2.8 Cd-NMR Night shift Tensor

In general, for two sites that change in a symmetry operation in NMR, the two sites produce equivalent resonance lines if the magnetic field direction does not change before and after the symmetry operation. Therefore, by measuring the shift of the resonance line of each site, information on the symmetry of the site can be obtained. This figure is the four Cd sites of pyrochlore lattice [14],which shows the angle dependence of the night shift measured by rotating the magnetic field in the I phase, I I phase, and II phase. The magnetic field was rotated in the $(11\bar{0})$ plane.

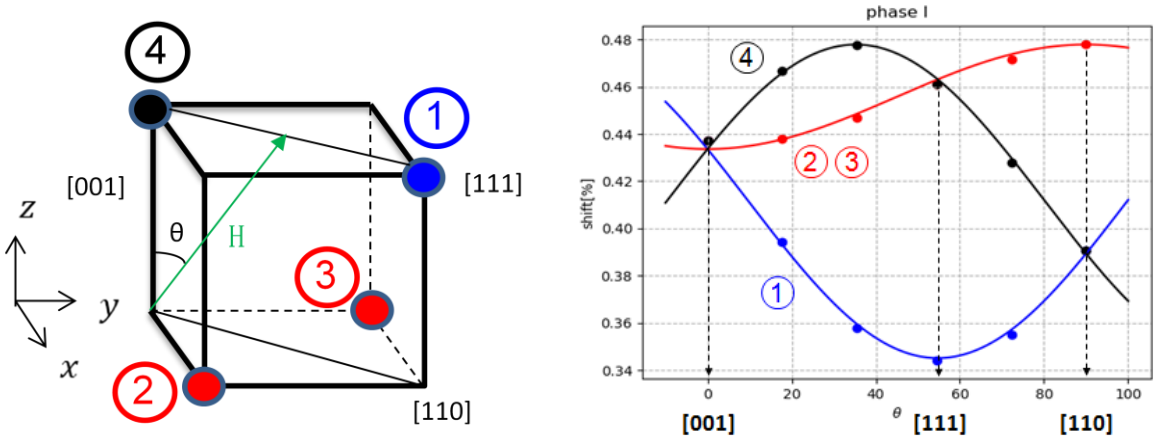

Fig.2.3 and Fig.2.4 Angle dependence of shift of phase I

For the symmetry of the Cd site in the pyrochlore compound Cd2Re2O7 is $D3d$, and Site shift tensors of Cd ① in the figure are classified by the irreducible representation of the high temperature phase $Fd\bar{3}m$. Consider the symmetry of $D3d$, each Cd site has a different main axis direction and and is converted to C_{2x} as： Cd ① ⟹ Cd ②, C_{2y} ： Cd ① ⟹ Cd ③, C_{2z}： Cd ① ⟹ Cd ④. Hamiltonian of Hyperfine interaction H_{hf} is given as

$$\mathcal{H}hf=\boldsymbol{IKB}^T=\Sigma K_{\alpha\beta}I_\alpha B_\beta \quad (\alpha,\beta=\mathrm{x, y, z}) \qquad (25)$$

where $\boldsymbol{I}$ = (Ix, Iy, Iz) is the nuclear spin, $\boldsymbol{B}$ = (Bx, By, Bz) is the external magnetic field, $\boldsymbol{K}$ is the shift tensor.

There is conversion law as: C_3[111]: Ix ⟹ Iy ⟹ Iz . m$(1\bar{1}0)$: Ix ⟹-Iy, Iy⟹ -Ix, Iz ⟹ -Iz.

Expressing this combination as a shift tensor, it is expected that the night shift in phase I will be represented by two parameters, a and b. So the Irreducible representation of K (Cd①) can be given as:

$$K(\mathrm{A}_1^{\mathrm{a}}\mathrm{g}) = \begin{pmatrix} \mathrm{a} & 0 & 0 \\ 0 & \mathrm{a} & 0 \\ 0 & 0 & \mathrm{a} \end{pmatrix} \tag{26}$$

$$K(\mathrm{A}_1^{\mathrm{b}}\mathrm{g}) = \begin{pmatrix} 0 & \mathrm{b} & \mathrm{b} \\ \mathrm{b} & 0 & \mathrm{b} \\ \mathrm{b} & \mathrm{b} & 0 \end{pmatrix} \tag{27}$$

where $K(\mathrm{A}_1^{\mathrm{a}}\mathrm{g})$ $K(\mathrm{A}_1^{\mathrm{b}}\mathrm{g})$ means diagonal and off-diagonal in phase I.

The Cd ① site shift tensor can be obtained, but since the other three sites with different spindle directions also give their resonance lines, these shift tensors must also be considered. Cd ① site convert to Cd ②, ③, ④ site with double axis $C2x$, $C2y$, $C2z$ respectively. And the shift tensor of Cd ①, ②, ③, ④ is given as K1,K2,K3,K4:

$$\mathrm{K1} = \begin{pmatrix} \mathrm{Kxx} & \mathrm{Kxy} & \mathrm{Kxz} \\ \mathrm{Kyx} & \mathrm{Kyy} & \mathrm{Kyz} \\ \mathrm{Kzx} & \mathrm{Kzy} & \mathrm{Kzz} \end{pmatrix} \tag{28}$$

$$\mathrm{K2} = \begin{pmatrix} \mathrm{Kxx} & -\mathrm{Kxy} & -\mathrm{Kxz} \\ -\mathrm{Kyx} & \mathrm{Kyy} & \mathrm{Kyz} \\ -\mathrm{Kzx} & \mathrm{Kzy} & \mathrm{Kzz} \end{pmatrix} \tag{29}$$

$$\mathrm{K3} = \begin{pmatrix} \mathrm{Kxx} & -\mathrm{Kxy} & \mathrm{Kxz} \\ -\mathrm{Kyx} & \mathrm{Kyy} & -\mathrm{Kyz} \\ \mathrm{Kzx} & -\mathrm{Kzy} & \mathrm{Kzz} \end{pmatrix} \tag{30}$$

$$\mathrm{K4} = \begin{pmatrix} \mathrm{Kxx} & \mathrm{Kxy} & -\mathrm{Kxz} \\ \mathrm{Kyx} & \mathrm{Kyy} & -\mathrm{Kyz} \\ -\mathrm{Kzx} & -\mathrm{Kzy} & \mathrm{Kzz} \end{pmatrix} \tag{31}$$

To transform into the phase II, it is distorted from a cubic crystal to a tetragonal crystal. For the magnetic field was rotated in the $(11\bar{0})$ plane of the cubic crystal to perform the measurement. If the cubic a, b, c axes are given as x, y, z axes, assuming that the c axis directions of domains I, I I, and III are z, x, and y axes, the magnetic field vector at any angle of rotation θ and the surface of rotation of the magnetic field in each domain is given as :

Magnetic field direction in each domain

Domain	C-axis direction	Surface of revolution	Magnetic field
Domain I	**C//Z**	$(1\bar{1}0)$	$B(\frac{\sin\theta}{\sqrt{2}}, \frac{\sin\theta}{\sqrt{2}}, \cos\theta)$
Domain II	**C//X**	$(01\bar{1})$	$B(\cos\theta, \frac{\sin\theta}{\sqrt{2}}, \frac{\sin\theta}{\sqrt{2}})$
Domain III	**C//Y**	$(\bar{1}01)$	$B(\frac{\sin\theta}{\sqrt{2}}, \cos\theta, \frac{\sin\theta}{\sqrt{2}})$

Using the parament (a,b,c1,c2,d1,d2), there will be 12 NMR resonance lines of the angle dependence of the shift(3 domains and 4 sites).

Since there are a total of 6 symmetric components in the shift tensor, there are four combinations of c1, c2, d1 and d2 as shown here in addition to these two components, and the low temperature at which the symmetry of the crystal structure decreases. In the phase, these components can also take non-zero values. If a tetragonal structure is realized in Phase II and Phase III, it is expected that c1 and d1 will appear.

The angle dependence of knight shift in phase II (a=0.2434、b=−0.0491、$c1$=0.0068、$c2$=$d1$=$d2$=0) and phase III(a=0.1570、b=−0.0535、$c1$=−0.0046、$d1$=0.0027、$c2$=$d2$=0) :

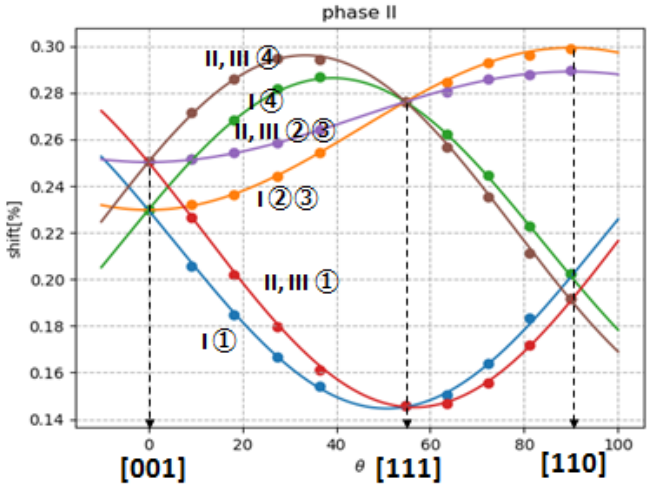

$$K_1^{Ea}(1) = \begin{pmatrix} c1 & 0 & 0 \\ 0 & c1 & 0 \\ 0 & 0 & -2c1 \end{pmatrix}$$

Fig.2.5 Angle dependence of shift of phase II

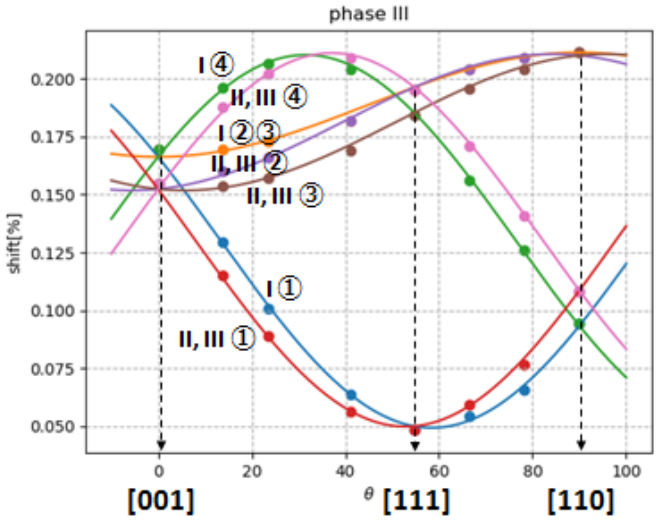

$$K_1^{Eb}(1) = \begin{pmatrix} 0 & -2d1 & d1 \\ -2d1 & 0 & d1 \\ d1 & d1 & 0 \end{pmatrix}$$

Fig.2.6 Angle dependence of shift of phase III

When phase II transform phase III, the resonance line on the high frequency side splits into two lines, means $c2 \neq 0$, and neither space group $I\bar{4}m2$ nor $I4_122$ allow this. This means an orthorhombic crystal, and this result suggests that there is an orthorhombic intermediate phase between the II phase and the III phase.

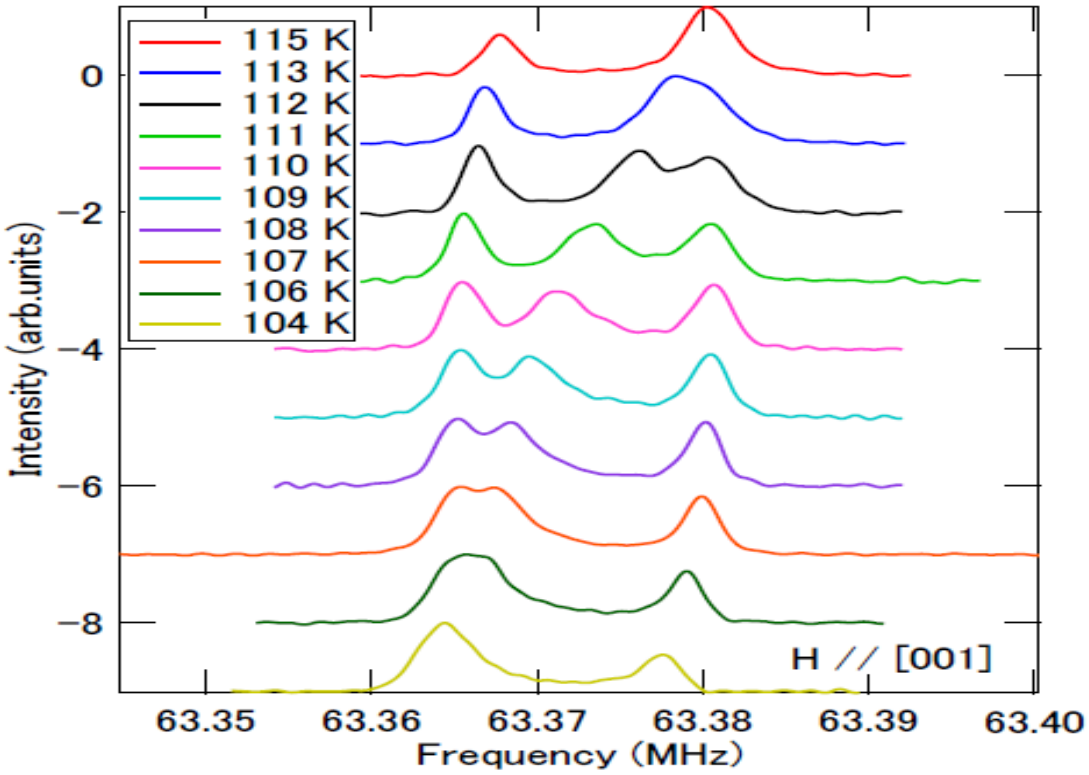

Fig.2.7 Temperature dependence near $Ts2$ of resonance line in direction [001]

Chapter.3

3.Results

3.1 Comparison and verification with previous experiments

Fig.3.1 and Fig.3.2 is one of the Cd- NMR spectra for B // [001] . Green line shows an irreversible change of the domain ratio at 180 ~ 170 K during the second cooling process from red line, which show that volume ratio of Z-domain and XY-domains has changed irreversibly during cooling down with the 17O enriched crystal. It is obvious that from the Fig 3.2 the intensity of peak has changed from 1:2 to 2:1.

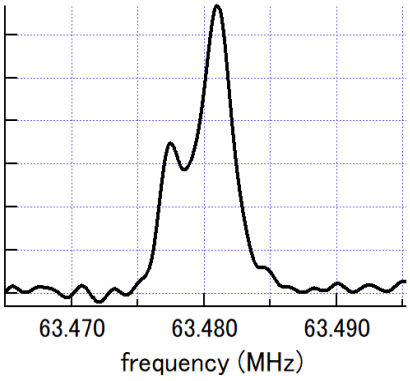

Fig.3.1 First crystal of Cd NMR spectra

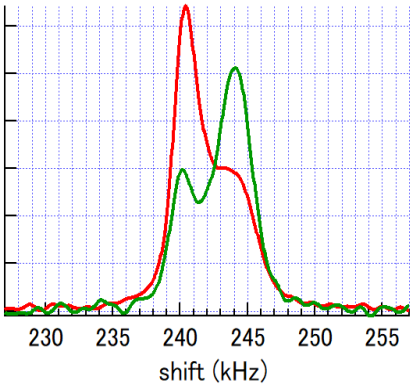

Fig.3.2 ^{17}O enriched crystal of Cd NMR spectra

Since there is one Cd site in the $F\bar{4}3m$ structure, Cd-NMR does not allow us to distinguish the $Fd\bar{3}m$ and the $F\bar{4}3m$ structures. However, the oxygen site located near the center of the Re-Re bonds should be split into two sites. Thus, we expect the O-NMR spectra to split into two peaks, should the $Fd\bar{3}m$ to $F\bar{4}3m$ transition occur. Therefore, we decided to perform O-NMR experiments. Single crystals of Cd_2Re2O7 enriched with 17O isotope with the nuclear spin 5/2 have been successfully synthesized and we are now conducting O-NMR measurements.

Fig3.3 is the ^{17}O NMR spectrum for B // [111] (T = 220K H = 7).There can observe two sets of NMR spectrum each of which consists of quarupole split five

lines. A total of 11 resonance lines are observed. Of these, the resonance line shown in green in the center is the signal from the O'site, and as expected, there is no quadrupole splitting and there is only one resonance line. In addition to this, two sets of five-split resonance lines are observed, which are divided into two non-equivalent groups of three O-sites by the magnetic field in the [111] direction, as shown here. It corresponds to the division.

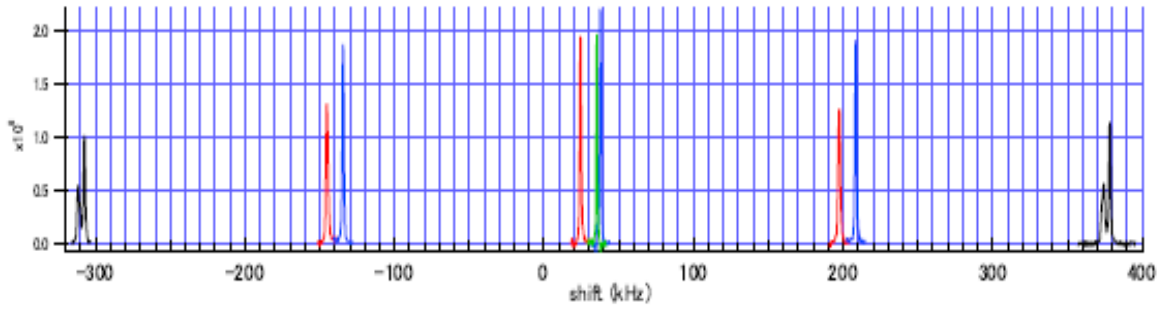

Fig. 3.3. ^{17}O NMR spectra for B // [111] (T = 220K H = 7)

Fig.3.4 is the NMR spectrum with the magnetic field applied along [001] direction. Comparing with the Fig.3.2 by N. Mera , it is successfully reproduced 17O enriched crystal NMR spectrum. In Fig.3.4, both OA(Blue) and OB(Red) site, which shown in Fig.3.5, is splitting into 5 sets. The center line of O’(Green) is in the middle, and then the 1st and 2nd lines split to both sides in turn. Under a magnetic field in the [001] direction, the 6 O-sites are divided into 2 and 4 non-equivalent groups as shown here. These are called OA sites and OB sites. From the intensity ratio of the resonance lines, the resonance lines shown in red can be assigned to the OB site and the resonance lines shown in blue can be assigned to the OA site. Of the five quadrupole split resonance lines, the center line is the center line, the resonance lines on either side of it are the low frequency and high frequency first satellites, and the resonance lines at both ends are the low frequency and high frequency first satellites. It is called 2 satellite. Below, we will look at how each resonance line splits due to the phase transition at Ts1. The following research of these three types of O NMR spectra when temperature decreases will based on Fig.3.4.

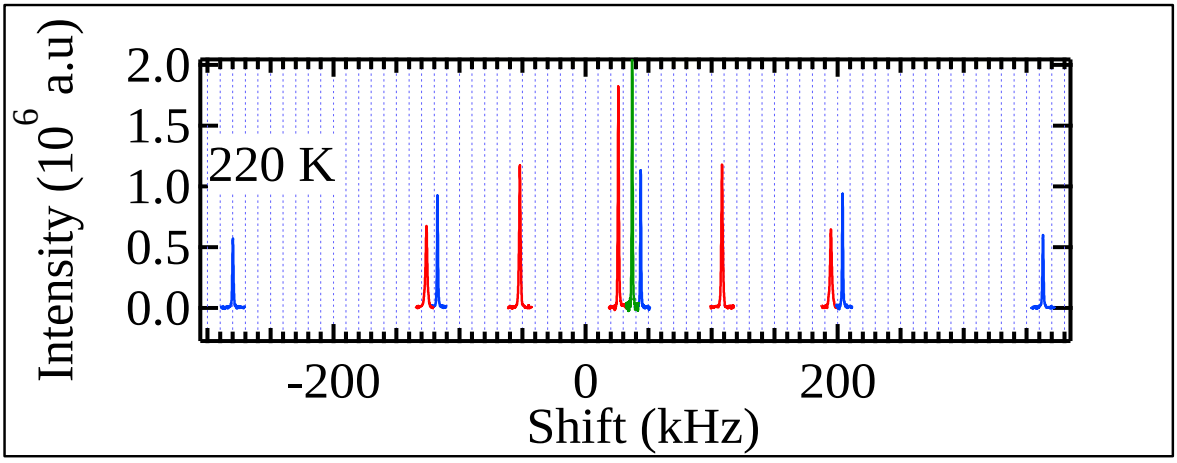

.

Fig.3.4 ^{17}O NMR spectra for B // [001] (T = 220K H = 7)

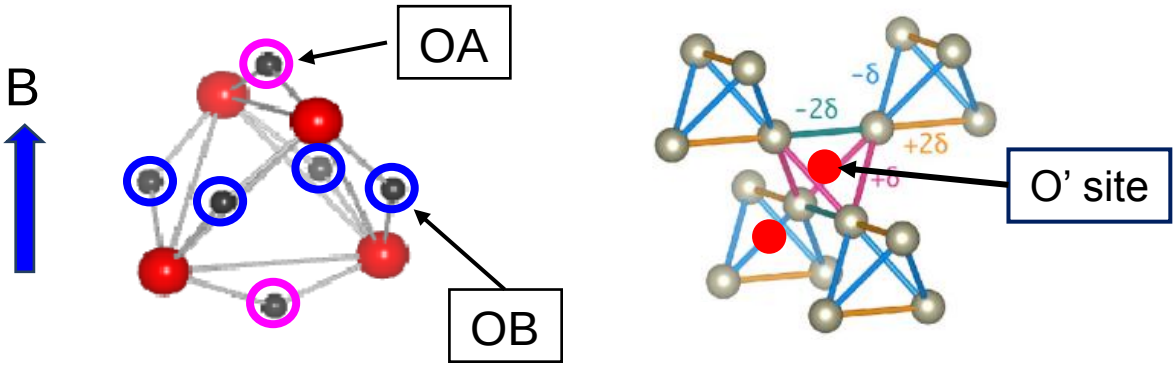

Fig. 3.5. Crystal structure of $Cd_2Re_2O_7$ B // [001]

From the oxygen spectra of the two magnetic field directions at 220K, the components of the O-site and O "site shift tensors, and the electric field gradient tensor were thus determined as:

O side

$$a = 6.45 \times 10^{-4}$$

$$b = 2.45 \times 10^{-4}$$

$$c = 1.05 \times 10^{-3}$$

$$\nu_a = 80.4 \text{ kHz}$$

$$\nu_b = 257.2 \text{ kHz}$$

O’ side

$$a = 9.2 \times 10^{-4}$$

3.2 NMR spectrum of O’

The temperature change of the spectrum of the centerline is shown as Fig 3.6.At 220K, one resonance line at each of the OA, OB, and O'sites shows splitting at a temperature lower than Ts1 = 203K. At least 4 peaks appear in OA and OB, and at least 3 peaks can be seen at the O'site. Considering the O'site, it has high symmetry at high temperatures. In phase I, the shift tensor had only one isotropic component and the electric field gradient tensor was zero, but in phase II, two components a and b appear on the diagonal elements, reflecting tetragonal symmetry. In this case, the formation of the domain is expected to result in two split resonance lines with an intensity of 1: 2. Furthermore, if the inversion symmetry is broken, it is expected that two sets of resonant lines split at an intensity of 1: 2 will appear because the two O'sites that change due to inversion at high temperature become unequal. Since the split resonance lines overlap at the center line, it is difficult to determine exactly how many resonance lines there are. Therefore, we will focus on the quadrupole satellite.$I\bar{4}m2$.

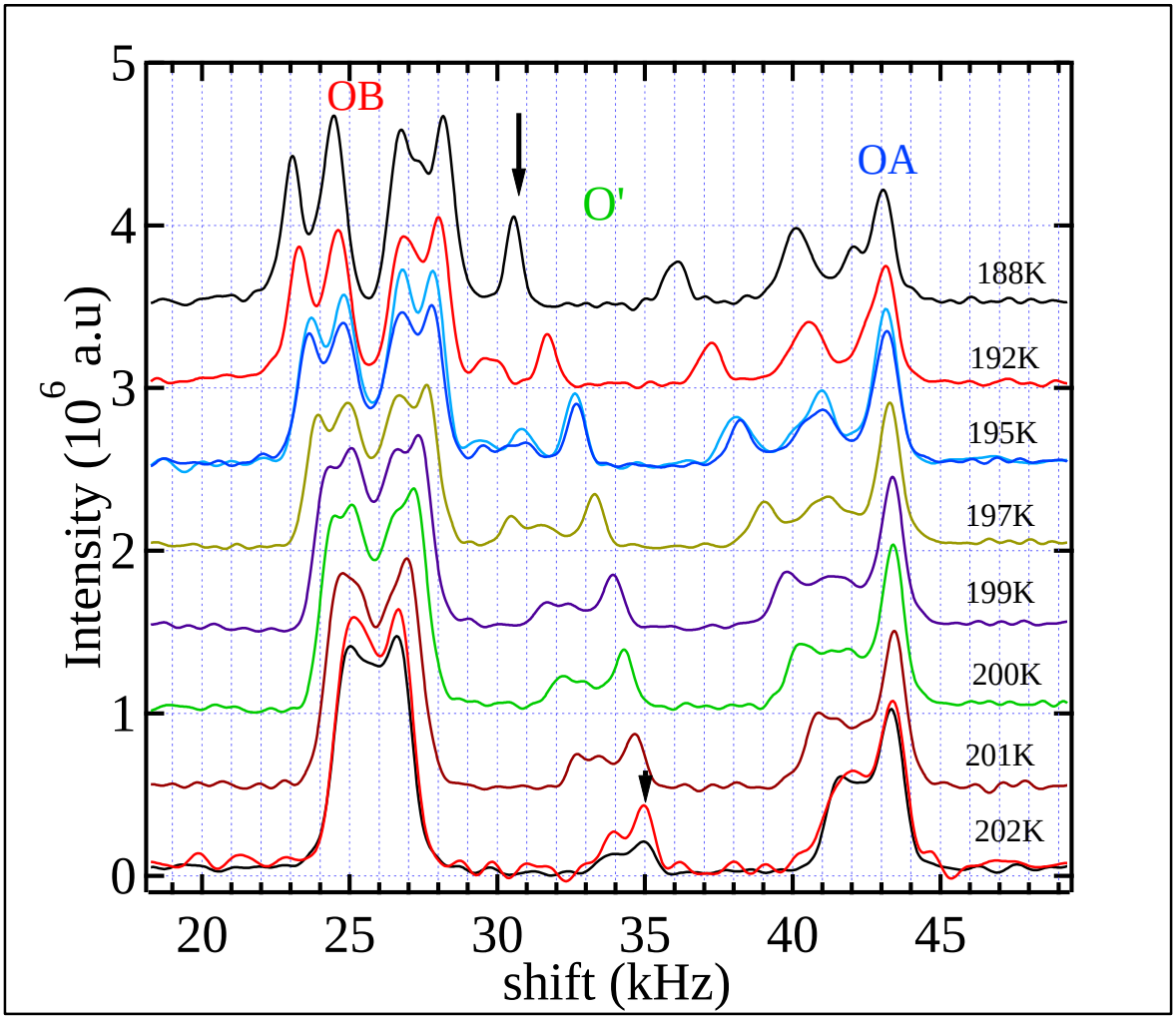

Fig. 3.6. ^{17}O' NMR spectra for B // [001]

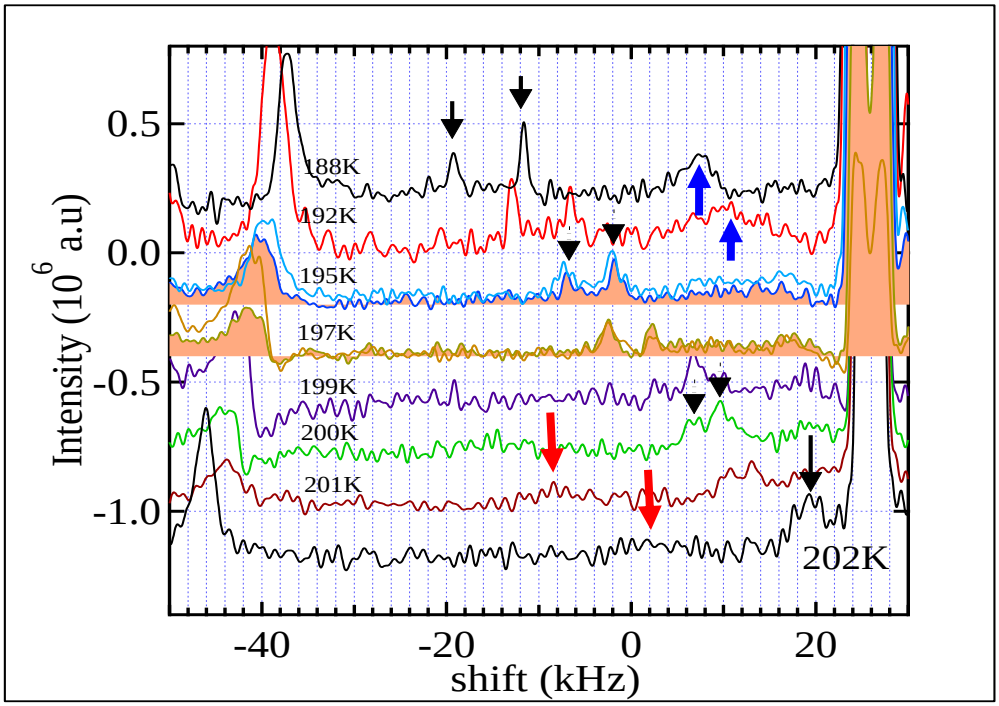

Fig. 3.7. O' NMR spectra for B // [001]

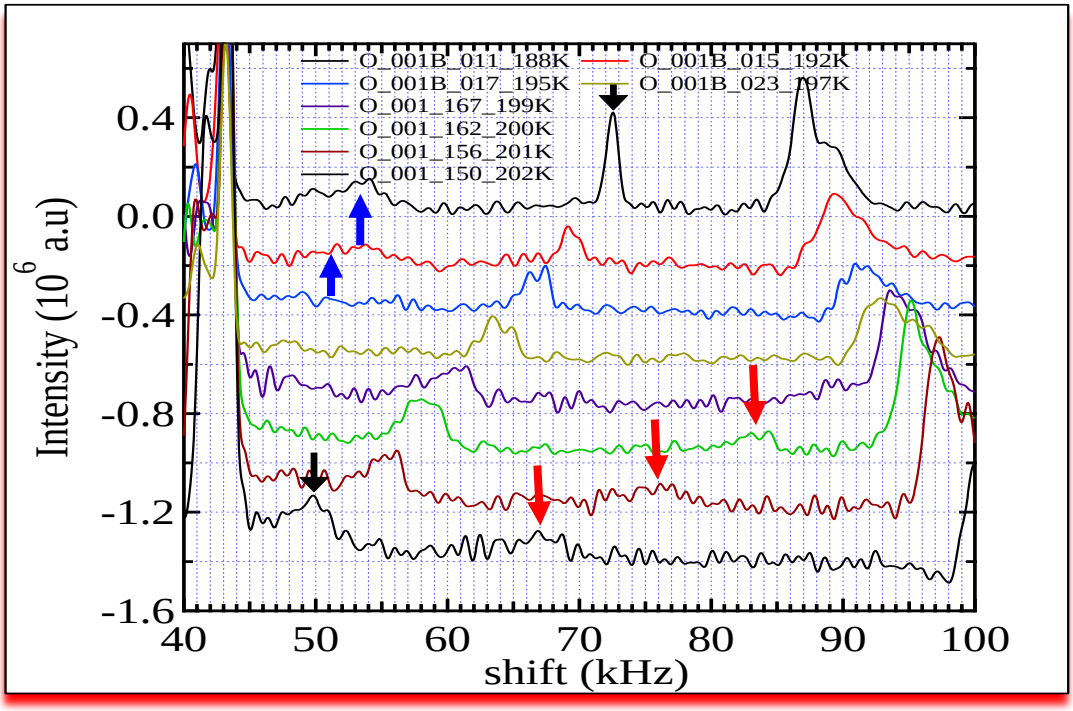

Fig. 3.8. O' NMR spectra for B // [001]

As shown by the arrows in Fig.3.7 and Fig.3.8, five quadrupole split resonance lines were observed at the O 'site at temperatures lower than Ts1. The split interval increases rapidly as the temperature decreases, which is consistent with the secondary phase transition at Ts1. Furthermore, as indicated by the black arrow, two sharp resonance lines appear in the low-frequency first satellite, which is thought to be due to the appearance of two types of sites with different electric field gradients due to the inversion symmetry being broken. I will. At low temperatures, a new satellite resonance line with a small split width, indicated by the blue arrow, appears, which is thought to be a signal from the domain where the c-axis of the tetragonal crystal is perpendicular to the magnetic field.

3.3 NMR spectrum of OA

The spectrum of the high frequency second satellite at the OA site is shown as Fig 3.10 and 3.11. Fig 3.9 shows an example of calculating the state of resonance line splitting assuming appropriate parameters. The resonance line of the OA site splits into four lines with an intensity ratio of 1: 2: 2: 1 at a temperature lower than Ts1. This corresponds to the appearance of two types of splitting into two with an intensity ratio of 1: 2 due to domain formation of the tetragonal structure due to inversion symmetry breaking. This situation was clearly confirmed by the low temperature spectrum obtained in the experiment.

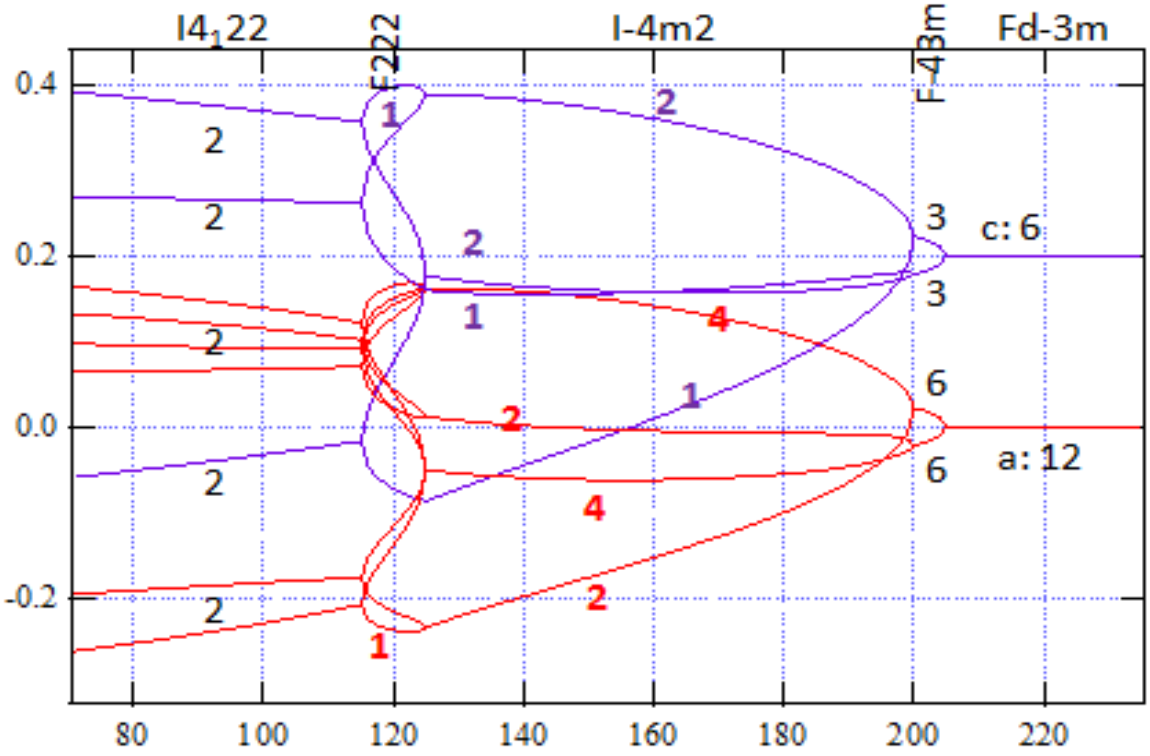

Fig. 3.9. Order Parameter (d(h_a) is finite)

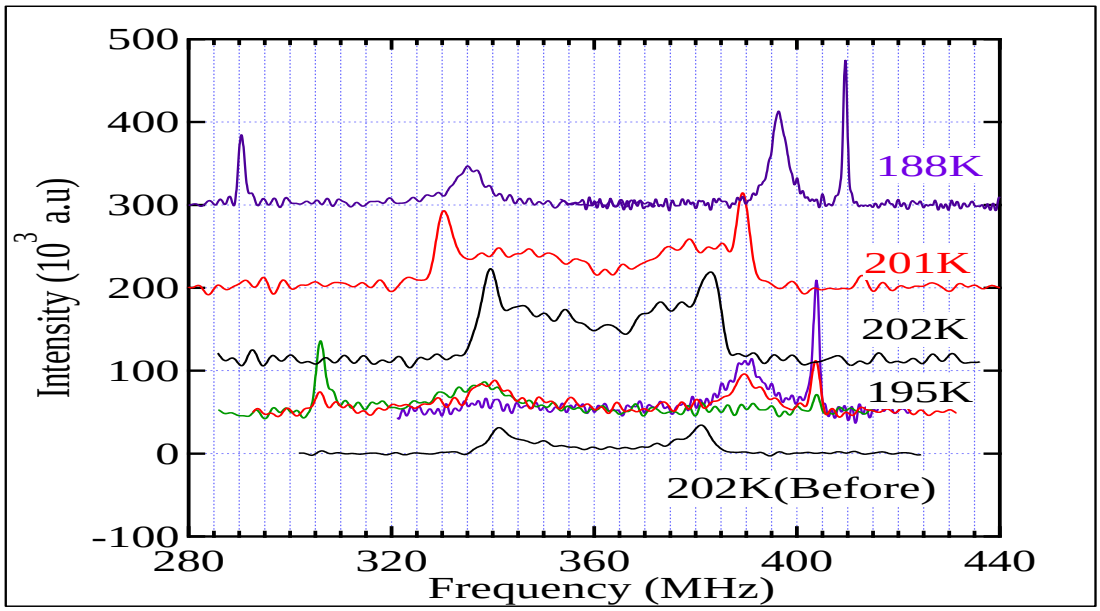

Fig. 3.10. OA NMR spectra for B // [001] OA 2nd

Similar spectral splitting was also observed in the low frequency second satellite spectrum of the OA site. The split interval of the satellite spectrum is more than 100 kHz, indicating that the lectron charge distribution changes significantly with the phase transition.

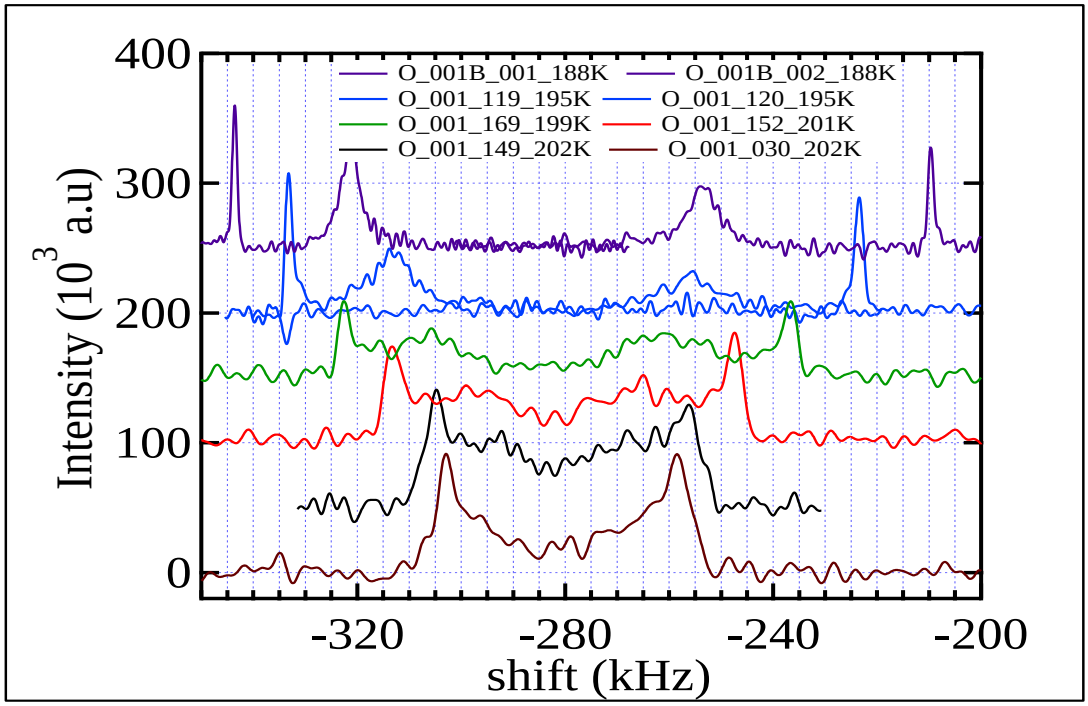

Fig. 3.11. OA NMR spectra for B // [001] (OA 2nd)

3.4 NMR spectrum of OB

From the Fig.3.12and Fig.3.13, the splitting of spectrum of OB spectrum can be obvious observed. It can be confirmed that it splits into at least 6 lines at 188K. The calculation result is 4: 2 2: 4 splits in fig 3.14 , which does not match the experiment. Further experiments are needed in the future.

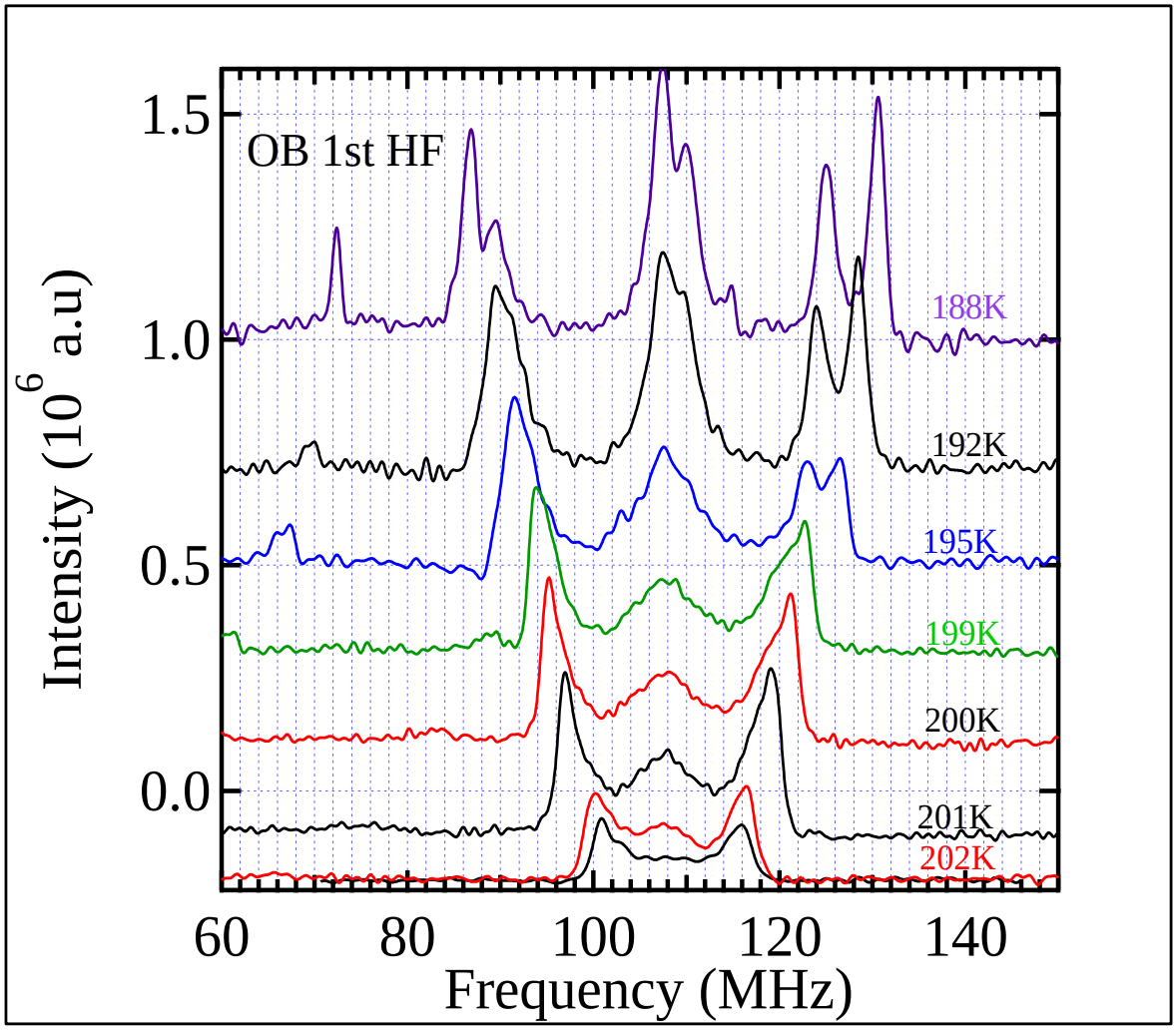

Fig. 3.12. OB NMR spectra for B // [001] (OB 1st)

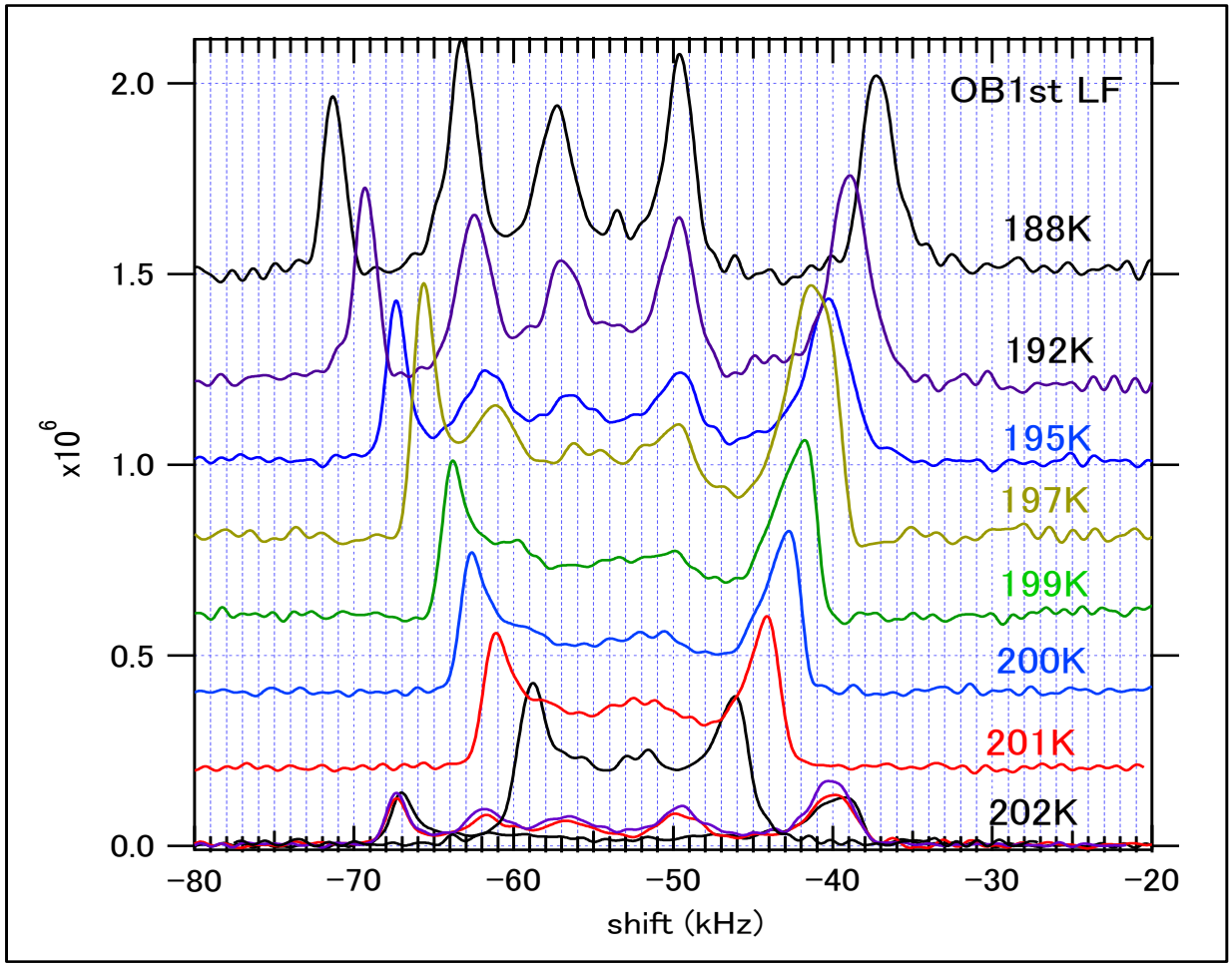

Fig. 3.13. OB NMR spectra for B // [001] (OB 1st)

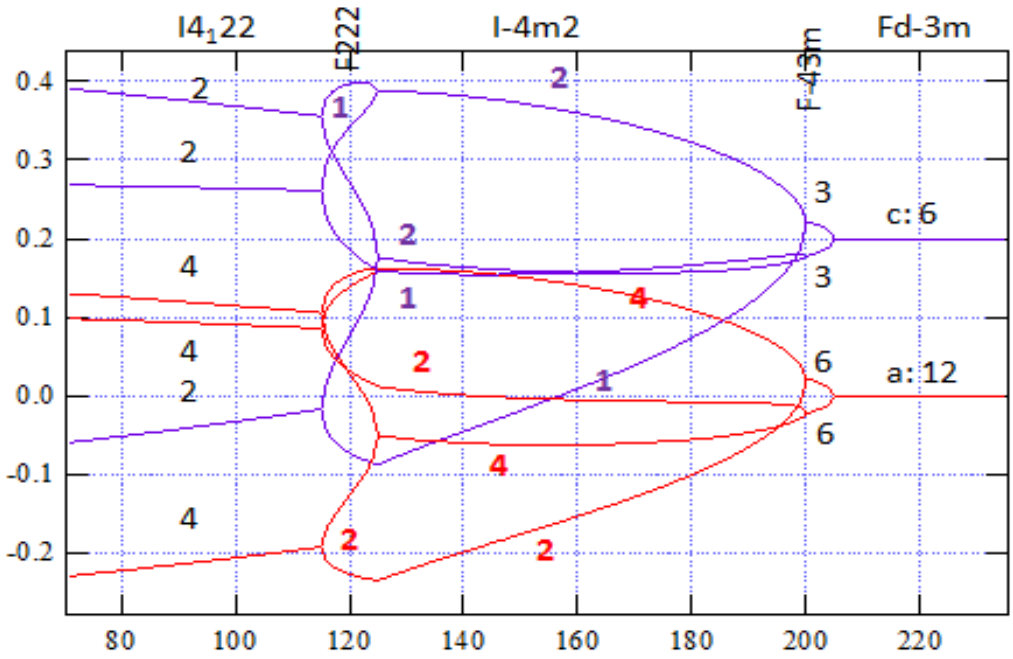

Fig. 3.14. Order Parameter(d=0)

Chapeter 4 Summary

In this reaserch , we measured NMR spectra of the ^{17}O enriched $Cd_2Re_2O_7$ crystal, and obtained 3 kinds of O resonance line near the temperature of Ts1=200K.which to further clarify the transformation of the crystal structure. In the high temperature I phase, the number of resonance lines expected from the crystal structure was observed.

Conclusion of O' NMR spectra

At lower temperatures than Ts1, five quadrupole split resonance lines were observed at the O'site. The split interval increases rapidly as the temperature decreases, which is consistent with the secondary phase transition at Ts1. Furthermore, as indicated by the black arrow, two sharp resonance lines appear in the low-frequency first satellite, which is thought to be due to the appearance of two types of sites with different electric field gradients due to the inversion symmetry being broken. The resonance line has an 1:2 split of resonance line intensity which should have no split, should be due to an electrical quadrupole. This is basically consistent with the previously speculated changes from the high-temperature cubic $Fd\bar{3}m$ to the low-temperature tetragonal

Conclusion of OA NMR spectra

The resonance line of the OA site splits into four lines with an intensity ratio of 1: 2: 2: 1 at a temperature lower than Ts1. This is as same as the example of calculating the state of resonance line splitting assuming appropriate parameters. Corresponding to the appearance of two types of splitting into two with an intensity ratio of 1: 2 due to domain formation of the tetragonal structure due to inversion symmetry breaking. This situation was clearly confirmed by the low temperature spectrum obtained in the experiment. Similar spectral splitting was also observed in the low frequency second satellite spectrum of the OA site. The split interval of the satellite spectrum is more than 100 kHz, indicating that the electron charge distribution changes significantly with the phase transition. resonance line, OA 1st spectra and OA 2nd spectra are Basically consistent with the order parameter, which shows the break of anti-symmetry.

Conclusion of OB NMR spectra

It can be confirmed that it splits into at least 6 lines at 188K. The calculation result is 4: 2 2: 4 splits, which does not match the experiment, need further experimentation and analyzed.

Future research

Under the magnetic field in the [001] direction, splitting of the resonance lines at the O', OA, and OB sites was observed in phase II, which is lower than Ts1. Since two types of quadrupole splitting occur at the O'site, the decrease in symmetry to tetragonal crystals and the breaking of inversion symmetry were directly verified. Tounderstand the splitting of the O-site resonant lines, we need further experiment, such as NMR measurement in *T*s2.

References

[1] J. S. Gardner, M. J. Gingras, and J. E. Greedan: *Reviews of Modern Physics* 82 (2010) 53.
[2] M. Hanawa, Y. Muraoka, T. Tayama, T. Sakakibara, J. Yamaura, and Z. Hiroi: *Physical Review Letters* 87 (2001) 187001.
[3] R. Jin, J. He, S. McCall, C. Alexander, F. Drymiotis, and D. Mandrus: *Physical Review* B64 (2001) 180503.
[4] H. Sakai, K. Yoshimura, H. Ohno, H. Kato, S. Kambe, R. E. Walstedt, T. D. Matsuda, Y.Haga, and Y. Onuki: *Journal of Physics: Condensed Matter* 13 (2001) L785.
[5] Z. Hiroi and J. Yamaura, *J. Phys. Soc. Jpn.* **71** (2002) 2598.
[6] Z. Hiroi, J. Yamaura, T. C. Kobayashi, Y. Matsubayashi, and D. Hirai, *Journal of the Physical Society of Japan*. **87** (2018) 024702.
[7] Liang Fu, *Phys. Rev. Lett.* **114** (2015) 026401.
[8] S. Hayami, Y. Yanagi, H. Kusunose, and Y. Motome, *Phys. Rev. Lett.* **122** (2019) 147602.
[9] Z. Hiroi, J.-I. Yamaura, Y. Muraoka, and M. Hanawa: *Journal of the Physical Society of Japan* **71** (2002) 1634.
[10] Y.Matsubayashi, Crystal growth and parity-breaking phase transitions of the spin-orbit-coupled metal $Cd_2Re_2O_7$.
[11] 川村光: (2016) 『重点解説スピンと磁性 2016 年 05 月号[雑誌] (数理科学別冊)』. サイエンス社.
[12] I. A. Sergienko and S. H. Curnoe: *Journal of the Physical Society of Japan* 72 (2003) 1607.
[13] Y. Ishibashi and M. Iwata: *Journal of the Physical Society of Japan* 79 (2010) 044604.
[14] N. Mera, M. Takigawa et al., unpublished.

Acknowledgments

I received a lot of help during this research.

As a guiding mentor, Professor Takigawa is a very rigorous academic professor. His thinking and attitude towards research have benefited me a lot. Professor Takigawa not only gave me a lot of guidance in experiments and research, but also often helped me in life. As a foreigner, during the two years studying abroad, I encountered a lot of difficulties and dealt with many things that were not comprehensive enough. But thanks to Professor Takigawa who has been supporting and helping me, I was able to move forward smoothly today. Professor Takigawa will be my mentor throughout my life.

Dr. PD Takeda is a serious and talkative seniors, which often provide me learning aids to my knowledge that is not well-founded. The secretary, Ms. Kawai ,manages the daily life of our laboratory and has allowed me to spend a very warm 2 years. The graduated Seniors Miss Ishikawa, Mr. Isomae, Mr. Yara and Mr. Watanabe can communicate patiently with me althought I am a foreigner. It is the honor of my life to be able to enter the Sichuan Laboratory.

Finally, I would like to express my sincere gratitude to all the family members who have supported us in a wide variety of ways since admission. Thank you to everyone for supporting me for two years.